

SURFACE PROPERTIES OF METAL OXIDES AND THEIR ROLE ON ELECTROCHEMICAL HYDROGEN STORAGE OF CARBON NANOTUBES

N. B. MKHONDO, T. MAGADZU*

University of Limpopo, School of Physical and Mineral Sciences, Department of Chemistry, Private Bag X 1106, Sovenga, 0727, South Africa

Herein, a variety of metal oxides nanoparticles were successfully doped on multi-walled carbon nanotubes (MWCNTs) by incipient-wetness method, and the structure of MWCNTs remained intact as confirmed by XRD data; their surface properties, as well as hydrogen storage were investigated. The data shows a decrease in BET surface area and macroporous volume of NiO, Co₃O₄ and Fe₂O₃-MWCNTs composites, as compared to that of acid treated MWCNTs (343.09 m²/g). This is linked with formation of large nanoparticles, that tend to block the MWCNTs passage as revealed by SEM and TEM images. Interestingly the CuO-MWCNTs showed an increase in surface area (558.04 m²/g), and mesoporous volume. This is well linked with small blade-like nanosheet of CuO within and on the surface of acid treated MWCNTs, as revealed by SEM and TEM data. The surface properties of CuO-MWCNTs correlated with high discharge capacity of 159 mAh/g (corresponding to 0.59wt% H₂ storage). Although, the discharge capacity values are low, the order of increase correlated with the surface area of the composite as follows: NiO-MWCNTs < Co₃O₄-MWCNTs < Fe₂O₃-MWCNTs < CuO-MWCNTs. The discharge capacity of CuO-MWCNTs composite is mainly attributed to the unique surface characteristics and existence of a synergetic interaction between CuO and MWCNTs. The data indicates the need of both mesoporous and macroporous structure of composites for effective hydrogen storage.

(Received February 9, 2018; Accepted October 6, 2018)

Keywords: CuO-MWCNTs composite, Electrochemical hydrogen storage, Discharge capacity, Surface properties, Metal oxides

1. Introduction

The increasing demand of high energy sources continues to attract more research and in particular a suitable hydrogen storage materials. Among various technologies [1], hydrogen technology has a potential of powering automobile and as stationary energy source with zero pollution of the environment [2], due to its high energy efficiency. However, for this to be realised a suitable storage material that is capable of storing and releasing hydrogen when needed has to be developed. Carbon nanomaterials such as CNTs continue to attract a wide spread scientific interest as one such suitable material due to their light-weight and tuneable surface properties. CNTs have shown potential as support material of metal and metal oxides, which are capable of altering their active surface area and electrical conductivity [3]. The combine effects of metal or metal oxides-MWCNTs hybrids open-up a wide variety of functionalities in areas such photocatalysis, supercapacitors, photovoltaic, lithium-ion batteries, sensor and hydrogen storage [4]. For examples, Pt-Ru/CNTs electrodes [5] have shown to exhibited excellent electro-catalytic activities for methanol electro-oxidation. Fe_{0.9}Co_{0.1}S₂/CNTs electrodes [6] are reported to be highly efficient catalyst for hydrogen generation.

Over the past five years a variety of 3d transition metal oxides (MO_x, M = Fe, Mn, Ni, Cu etc.) supported on carbon nanomaterials have been investigated for energy storage [1,6-8], with little reports on hydrogen storage [9-12, etc.]. For examples, a report on MWCNTs doped with TiO₂, [9] demonstrated an improved electrochemical hydrogen storage ability of the composite. A

*Corresponding author: takalani.magadzu@ul.ac.za

recent report on gaseous adsorption has indicated an increase in hydrogen storage from 0.09 to 0.9 wt.% upon decoration of MWCNTs by Co and Cu-oxide nanoparticles (at 25 °C and equilibrium hydrogen pressure of ~23 atm) [13]. The improved hydrogen storage was attributed to the hydrogen spill-over mechanism on the surface of MWCNTs [13], with the surface area of the composite decreasing with metal oxides addition. In related surface electrodes reactions, some previous studies [1,14] have indicated enhanced supercapacitive behaviour of NiO nanoflake electrode; that was attributed to their high surface area. These reactions depend on the kinetic properties of the electrodes; hence the nanoparticles with high surface area provide fast electron transfer process during charge/discharge cycles [15]. Furthermore, metal nanoparticles are known to act as redox sites, which lead to improved electrochemical hydrogen storage [16].

It was therefore, envisaged that different metal oxides nanoparticles can alter/influence the surface properties of MWCNTs. Hence, the investigation of electrochemical hydrogen storage mainly focus on the surface properties of the metal oxides doped on MWCNTs and their roles towards hydrogen storage activity of MWCNTs. Although few recent studies [10-12, etc.] have been reported on electrochemical hydrogen storage, none had investigated the effects of various metal oxides on the electrochemical hydrogen storage of MWCNTs.

2. Experimental

2.1 Preparation of acid-treated MWCNTs

Prior to metal oxides (NiO, Co₃O₄, Fe₂O₃ and CuO) addition, MWCNTs (Sigma Aldrich) were acid treated using a mixture of H₂O₂ and HNO₃ in a ratio of 1:3 (v/v) respectively, as described elsewhere [17].

2.2 Preparation of metal oxide on acid-treated MWCNTs

Approximately 20 g of metal nitrate precursors, (i.e Ni(NO₃)₂·6H₂O; Co(NO₃)₂·6H₂O; Fe(NO₃)₃·9H₂O; and Cu(NO₃)₂·6H₂O) were calcined at 300 °C for 2 h under air atmosphere; resulting in the formation of NiO, Co₃O₄, Fe₂O₃ and CuO nanoparticles. Approximately 5 wt.% of prepared metal oxides were mixed with 0.2 g A-MWCNTs and 4 ml of *N,N*-Dimethylformamide as the binder. The mixture was sonicated for 15 min to allow the metal oxides to be well coated/dispersed on the surface of A-MWCNTs. The mixture was allowed to dry at room temperature overnight to allow the solvent to evaporate.

Finally, the detailed structures and the chemical compositions of acid-treated MWCNTs and metal oxides doped MWCNTs were characterised using Thermogravimetry Analysis (TGA), X-Ray Diffraction (XRD), Brunauer-Emmett-Teller (BET) surface area analysis and Transmission Electron Microscopy (TEM) and Scanning Electron Microscopy (SEM).

2.3 Preparation of electrodes and their electrochemical measurements

Approximately 35 mg of the composites were used to fabricate the glassy carbon working electrode following similar procedure described elsewhere [17]. The experiments were carried out on a Bioanalytical Systems Inc. (BASi) potentiostat driven by the epsilon EC (version 1.60.70), using a three-electrode system consisting of a glassy carbon electrode (GCE, 3.0 mm diameter) as working electrode, Ag/AgCl (saturated NaCl solution) as reference electrode and platinum wire as auxiliary electrode. Runs were carried out in a potential window of -1.4 to 0.2 V vs Ag/AgCl at a scan rate of 50 mV/s, using a 6 M KOH as the electrolyte. The prepared working electrodes were charged and discharged at a constant current of 3 mA.

3. Results and discussion

3.1 Characterisation

3.1.1 SEM analysis of NiO, Co₃O₄, Fe₂O₃ and CuO nanoparticles

Fig. 1 shows the SEM images of NiO, Co₃O₄, Fe₂O₃ and CuO nanoparticles prepared by calcination of respective precursors at 300 °C for 2 h. The image shows small and large particles of hexagonal-like geometry of NiO nanoparticles [Fig.1(a)]. The geometry of the prepared NiO

nanoparticles differs from the flake-like morphology reported elsewhere [18,19]. The SEM image of Co_3O_4 shows nanoparticles with fluffy-like morphology, which is arranged randomly to form a relatively loose packed microstructure [Fig.1(b)]. These particles differs from the Co_3O_4 nanoparticles prepared by solution combustion process [20], and in-situ chemical co-precipitation in alkaline solution [21]. A nanotubular structure of Fe_2O_3 can be seen on the SEM image [Fig.1(c)], as reported elsewhere, [2] during the preparation of $\alpha\text{-Fe}_2\text{O}_3$ through an anodization method on iron films. The authors demonstrated that the unique nanostructures of $\alpha\text{-Fe}_2\text{O}_3$ nanotube arrays provide high surface area, fast ion transport pathways and robust structures [2]. Lastly, the SEM image shows the CuO clusters with thin nanosheets [Fig.1(d)]. Similar morphology was reported elsewhere, [22] on CuO prepared by Chemical bath deposition method.

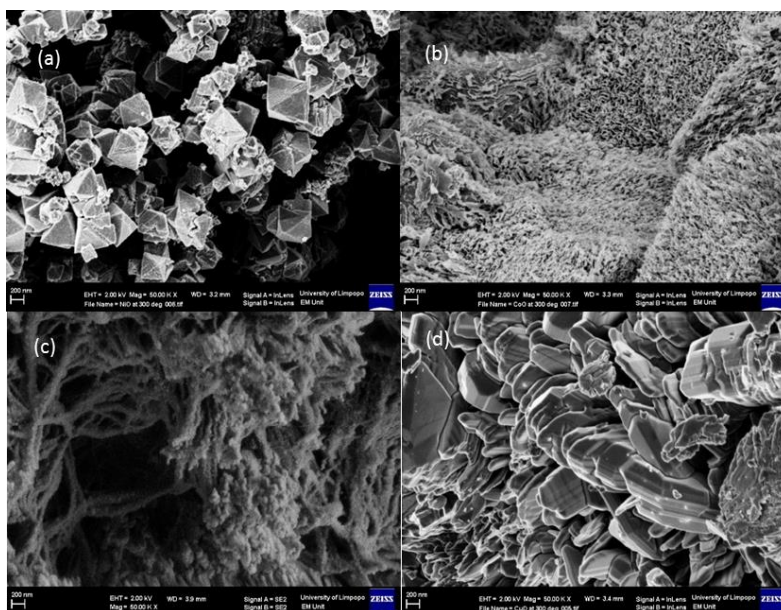


Fig. 1. SEM images of (a) NiO, (b) Co_3O_4 (c) Fe_2O_3 and (d) CuO nanoparticles.

3.1.2 TEM analysis of 5wt.% CuO-MWCNTs, 5wt.% Fe_2O_3 -MWCNTs, 5wt.% NiO-MWCNTs and 5wt.% Co_3O_4 -MWCNTs

The data in Fig. 2 show the TEM images of 5wt.% CuO-MWCNTs, 5wt.% Fe_2O_3 -MWCNTs, 5wt.% NiO-MWCNTs and 5wt.% Co_3O_4 -MWCNTs composites. The images shows that most of the CuO particles are within the structure of MWCNTs [Fig 2(a1)], although occasionally some few large particles are observed on the surface [Fig 2(a2)]. Low magnification TEM images do not show formation of any noticeable aggregates [Fig 2(a2)], although some of the CuO deposits has blocked the inner tubes of MWCNTs. The diameter of the CuO particles measured from the high magnification TEM ranged between 7-9 nm [Fig 2(a2)]. The Fe_2O_3 nanoparticles on MWCNTs [Fig 2(b1 & b2)], are dispersed similar to CuO, however large particles of Fe_2O_3 can be seen with an approximate particle size of 10-15 nm [Fig 2(b2)]. The TEM images of NiO [Fig 2(c1 & c2)] and Co_3O_4 [Fig 2(d1 and d2)] nanoparticles shows the dispersion of smaller particles embedded within the walls of MWCNTs, with particle sizes of 10-14 and 9-15 nm, respectively.

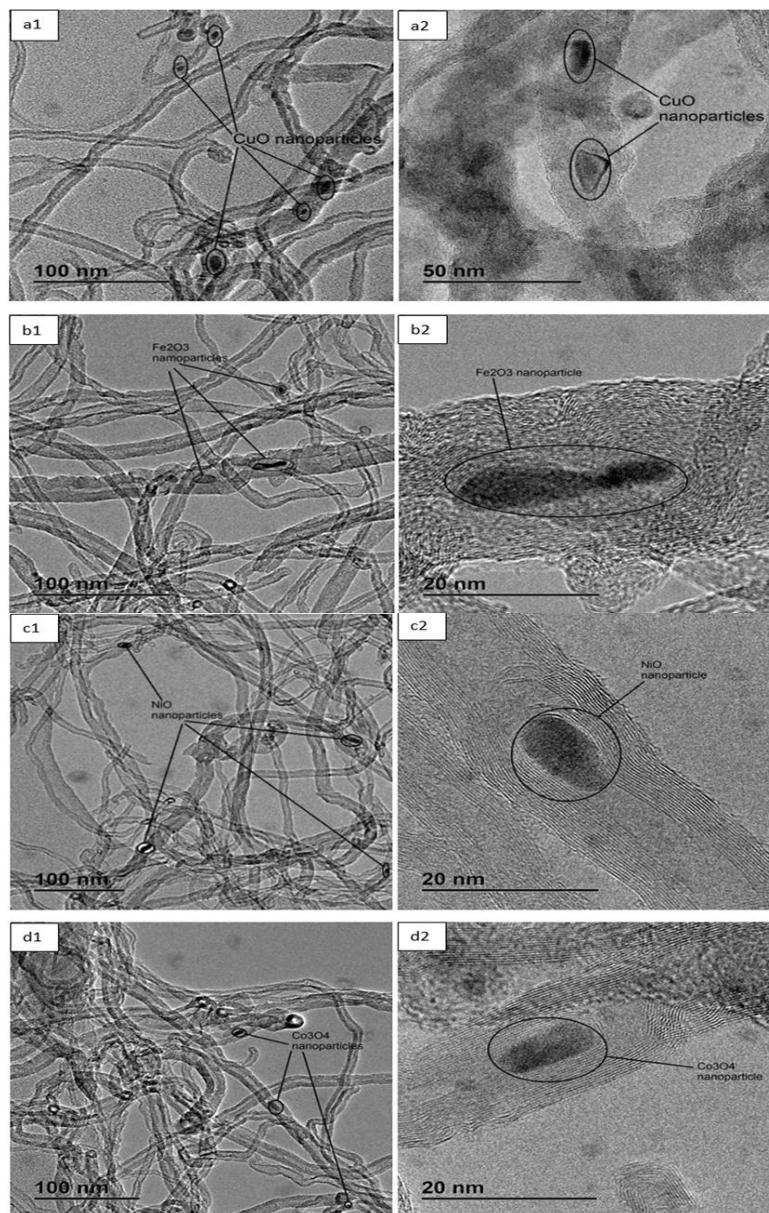


Fig. 2. TEM images of (a1) 5wt.% CuO-MWCNTs, (b1) 5wt.% $\text{Fe}_2\text{O}_3@300^\circ\text{C}$ -MWCNTs, (c1) 5wt.% NiO@300 $^\circ\text{C}$ -MWCNTs, and (d1) 5wt.% $\text{Co}_3\text{O}_4@300^\circ\text{C}$ -MWCNTs and their corresponding higher magnifications (a2,b2,c2,d2).

3.1.3 XRD analysis of 5wt.% NiO, CuO, Fe_2O_3 , and Co_3O_4 on MWCNTs nanocomposite

All metal oxides composites, showed the presence of graphitic carbon peak at 26° two theta, indexed to (002) plane characteristic of MWCNTs structure (Fig. 3). The data in Fig. 3(b) shows the XRD patterns of 5wt.% CuO-MWCNTs nanocomposite which can be well indexed to monoclinic copper oxide (CuO) phase [3]. No characteristic peaks assigned to impurities such as $\text{Cu}(\text{OH})_2$ or Cu_2O were detected. The average crystallite size calculated using the Scherrer's equation from the (111) peak is 19.73 nm for CuO-MWCNTs. This clearly suggests that the CuO nanoparticles were restricted to a specific size as soon as they are attached to or within the MWCNTs structure. This crystallite size is relatively similar to 19.83 nm observed on Cu-oxide/MWCNTs composites [13], even though the composites preparation differs. The iron oxide on MWCNTs is characteristic of Fe_2O_3 [23], with no impurities detected [Fig. 3(c)] and the calculated average crystallite size is 25.8 nm. The diffraction pattern of 5wt.% NiO-MWCNTs

confirms the formation of rock-like polycrystalline structure of NiO [18,24], as seen on the SEM images in figure 1, with average crystallite size of 20.2 nm [Fig. 3(d)]. Small NiO crystallite sizes were observed inside MWCNTs, due to walls restrictions. The XRD pattern of 5wt.% Co_3O_4 -MWCNTs composites, is in good agreement with the cubic phase of Co_3O_4 [21], with the average crystallite size from the (311) peak of 42.5 nm. This particle size differs to 26.13 nm, observed on Co-oxide/MWCNTs composite [13]. The crystallite size of all metal oxides remained low once attached to MWCNTs or inside the walls of MWCNTs structure.

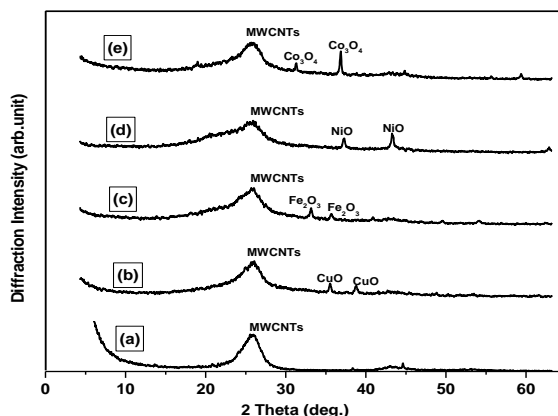


Fig. 3. XRD patterns of (a) Acid-treated MWCNTs, (b) 5wt.% CuO-MWCNTs, (c) 5wt.% Fe_2O_3 -MWCNTs, (d) 5wt.% NiO-MWCNTs and (e) 5wt.% Co_3O_4 -MWCNTs composites.

3.1.4 BET Surface area and pore volume analysis of acid-treated MWCNTs and metal oxides (NiO, Co_3O_4 , Fe_2O_3 and CuO) additives on MWCNTs

Fig. 4 depicts N_2 adsorption-desorption isotherm of the acid treated MWCNTs and various metal oxides (NiO, Co_3O_4 , Fe_2O_3 and CuO) additives on MWCNTs composites. The isotherms indicate the adsorption hysteresis behaviour in the $P/P_0 \sim 0.4$ to 0.99, with a mixture of mesoporous and macroporous structure. The data shows a decrease in BET surface area and macroporous volume of NiO, Co_3O_4 and Fe_2O_3 -MWCNTs composites (Table 1), with NiO-MWCNTs seriously affected, due to mesopores decrease. This is linked with large particle sizes of metal oxides that exists within the walls of carbon nanotubes, that seems to have blocked the tube pores (as confirmed by TEM data), and hence decreases the surface area of the entire composite. Similar findings were reported on Ni/SWCNTs [16] and Co_3O_4 /MWCNTs [13] composites. The surface area decreased from $584.8 \text{ m}^2/\text{g}$ for the as-prepared SWCNTs to $436.0 \text{ m}^2/\text{g}$ for 12 wt.% Ni-SWCNT [16], and from $310.0 \text{ m}^2/\text{g}$ for the pristine MWCNTs to $147.0 \text{ m}^2/\text{g}$ for 44 wt.% Co_3O_4 -SWCNT [13]. Zhang *et al.* [25] also reported a decrease in the BET surface area for acid-treated CNTs from 122.41 to $7.41 \text{ m}^2/\text{g}$ for 80wt.% MnO_x /CNTs.

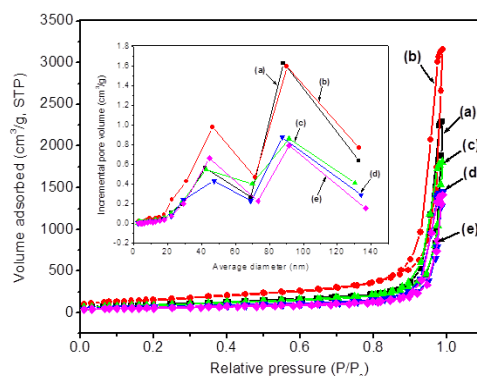


Fig. 4. N_2 adsorption and desorption isotherms and BJH pore size distribution of (a) acid-treated MWCNTs (b) 5wt.% CuO-MWCNTs (c) 5wt.% Fe_2O_3 -MWCNTs (d) 5wt.% NiO-MWCNTs and (e) 5wt.% Co_3O_4 -MWCNTs.

Interestingly to note is that the CuO-MWCNTs composite showed an increase in the surface area (558.04 m²/g), and mesoporous volume as compared to that of acid treated MWCNTs (343.09 m²/g, Table 1) and other composites. The mesopores enhancement is attributed to the coating of smaller nanosheets of CuO onto the surface of MWCNTs, which generates abundant pores [22]. This data contradict with the recent report [13], which indicated a decrease in BET surface area of CuO-MWCNTs composite prepared by in-situ reduction method.

Table 1. Surface characteristics of the metal oxides-MWCNTs samples determined from nitrogen physisorption at -195.8 °C.

Sample name	BET surface area (m ² g ⁻¹)	Peak pore volume (cm ³ g ⁻¹)	Peak pore sizes (nm)	Discharge capacity ¹ (mAhg ⁻¹)
A-MWCNTs	343.09	2.91	33.96	72.63
CuO-MWCNTs	558.04	4.11	29.48	158.84
Fe ₂ O ₃ -MWCNTs	330.27	2.38	28.87	112.78
Co ₃ O ₄ -MWCNTs	281.78	2.41	34.20	90.13
NiO-MWCNTs	237.58	1.97	33.11	89.91

¹All discharge capacity data were repeated three times at a constant current of 3 mA.

3.1.5 TGA analysis of Acid-treated MWCNTs and metal oxides (NiO, Co₃O₄, Fe₂O₃ and CuO) additives on MWCNTs

The TGA profiles measured in flowing air for Acid-treated MWCNTs and metal oxides (NiO, Fe₂O₃ and CuO) additives on MWCNTs are shown in figure 5(A). All metal oxide-MWCNTs composites exhibited one weight loss step in the range of 500-700 °C, which indicates the MWCNTs gasification [13]. The DTG curves shows various broad peaks, with maximum weight losses occurring at 637 °C, 613 °C, 644 °C and 654 °C for MWCNTs, CuO-MWCNTs, NiO-MWCNTs and Fe₂O₃-MWCNTs nanocomposites, respectively [Fig 5(B)]. This suggests a slow gasification of MWCNTs and metal oxide-MWCNTs composites, which is linked with the strength of the nanostructure of peroxide-nitric acid-treated MWCNTs [17]. In the range of 600 - 700 °C, a slight increase in stability of NiO and Fe₂O₃-MWCNTs is noted, with a decrease in CuO-MWCNTs, in relation to the peak maxima of acid treated MWCNTs which occurred at 637 °C [Fig 5(B)]. The metal oxide-MWCNTs composites shows the maximum weights losses of between 93 to 95%, indicating that the residual weight is predominantly metal oxides at approximately 5wt.% on MWCNTs [Fig 5(A)]. This loading is 9 times lower than that reported on cobalt oxide/MWCNTs, and copper oxide/MWCNTs composite [13].

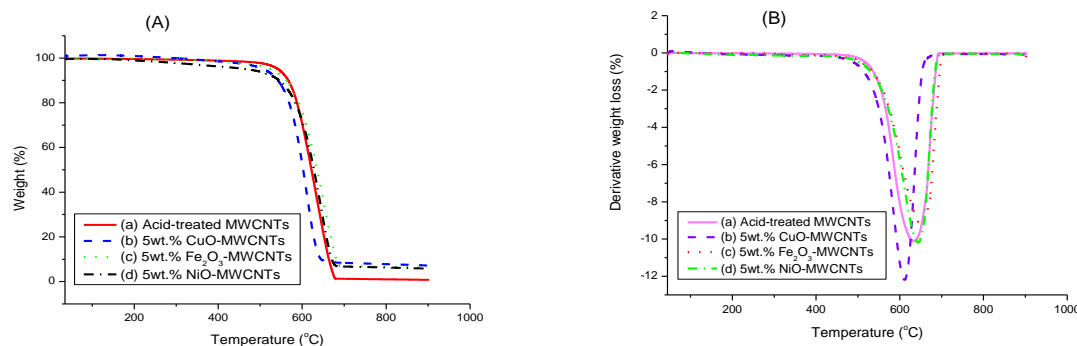


Fig. 5. TGA (A) and DTG (B) profiles of (a) acid-treated MWCNTs (b) 5wt.% CuO-MWCNTs (c) 5wt.% Fe₂O₃-MWCNTs and (d) 5wt.% NiO-MWCNTs.

3.2. Electrochemical hydrogen storage measurements

3.2.1 Cyclic voltammetric characteristics of acid treated MWCNTs and metal oxides doped MWCNTs electrodes

Fig. 6 shows the cyclic voltammograms (CV) curves of A-MWCNTs, 5wt.% CuO-MWCNTs, 5wt.% Fe₂O₃-MWCNTs, 5wt.% NiO-MWCNTs and (e) 5wt.% Co₃O₄-MWCNTs at potential interval of 0.2 to -1.4 V vs Ag/AgCl, scan rate of 50 mV/s. Interesting to note is that all curves displayed a rectangular shape, indicating a typical double-layer capacitive behaviour [26,27]. This behaviour differs from that reported elsewhere [9] on TiO₂ doped MWCNTs. The dissolved ions are accumulated at the M-MWCNTs (M = Metal oxides)/electrolyte interface by electrostatic attraction forces. The negative current reflects the number of hydrated potassium ions that accumulated during the cathodic polarization of the MWCNTs, while the positive current during anodic polarization corresponds to desorption of hydrated potassium ions [28]. The cathodic peaks at around -0.2 to -0.8 vs Ag/AgCl are attributed to hydrogen adsorption on metal oxides-multi-walled carbon nanotubes (M-MWCNTs) composites, in accordance with equation 1. The anodic peaks at around -1.0 to 0.0 V vs Ag/AgCl at opposite direction are attributed to oxidation of hydrogen adsorbed on M-MWCNTs composites. The peaks suggest in addition to capacitive behaviour, the faradaic reaction contributed to the measured discharge capacity [29]. Interestingly, no peak profiles were observed on acid treated MWCNTs, which indicates that adsorption of hydrogen occurred at lesser active sites; mainly those created by acid treatments.



The apparent cathodic peak of 5wt.% CuO-MWCNTs composite [Fig. 6(b)] at around -0.58 V (vs Ag/AgCl), gave a highly improved discharge capacity as compared to A-MWCNTs alone. The discharge capacity increased from 72.63 to 158.84 mAh/g in the order of A-MWCNTs < NiO-MWCNTs < Co₃O₄-MWCNTs < Fe₂O₃-MWCNTs < CuO-MWCNTs; and their corresponding electrochemical hydrogen storage are as indicated in figure 7. Interestingly, the high hydrogen adsorption of CuO-MWCNTs composite correlated with the higher BET surface area (558.04 m²/g) and increased mesoporous structure as compared to acid treated MWCNTs (343.09 m²/g) and all other metal oxides-MWCNTs composites (Table 1). The low discharge capacity values of Co₃O₄ and Fe₂O₃-MWCNTs composites is linked with a decrease in macropores volume as depicted by BET data. It is further worth noting the existence of a synergetic interaction between CuO and MWCNTs, since the discharge capacity of both CuO (-16.65 mAhg⁻¹) and MWCNTs (72.63 mAhg⁻¹) are lower than that of the composite system. The data further suggests that CuO provided more active sites on the surface of MWCNTs, similar to the role played by ZnO on alloy system [30]. The performance of CuO-MWCNTs composites is well linked with hydrogen spill-over onto the surface of MWCNTs [13], which facilitated the charge transfer on the surface of MWCNTs and the diffusion of hydrogen atoms from the surface to the inside of CNTs, which enhanced the dynamic property of CNTs in adsorption and desorption process. Furthermore, the discharge capacity of 159 mAh/g of 5 wt.% CuO on MWCNTs (which correspond to 0.59wt.%

hydrogen storage), is much higher than that reported on cobalt oxide/MWCNTs, and copper oxide/MWCNTs composite [13], in terms of mass ratio of dopants on MWCNTs.

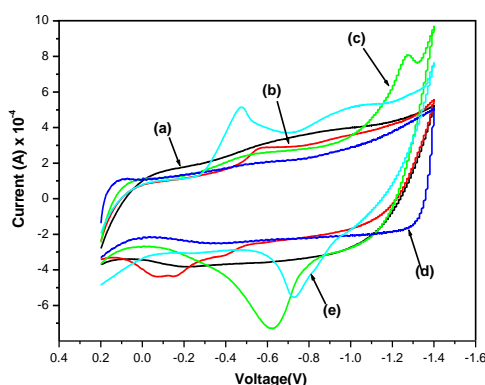


Fig. 6. CV curves of (a) A-MWCNTs (b) 5wt.% CuO-MWCNTs, (c) 5wt.% Fe_2O_3 -MWCNTs, (d) 5wt.% NiO-MWCNTs and (e) 5wt.% Co_3O_4 -MWCNTs.

Contrary to CuO-MWCNTs composites data, the 5wt.% NiO-MWCNTs composite [Fig. 6(d)] gave poor discharge capacity value (Table 1). The capacity correlated with the low BET surface area ($237.58 \text{ m}^2/\text{g}$), in relation to acid treated MWCNTs ($343.09 \text{ m}^2/\text{g}$) and hence; low electrochemical hydrogen storage (Figure 7). This indicates that the octahedral geometry of NiO has contributed to the blockage of electron passage within the MWCNTs, as shown by TEM images of 5wt.% NiO-MWCNTs. Other studies have indicated a formation of flake-like NiO particles, with high porous structure which is reported to permit easy access for solvated ions to the electrode/electrolyte interface [18,19]. This clearly indicates that the structure of NiO particles is dependent on the preparation method and influences the surface faradaic reactions.

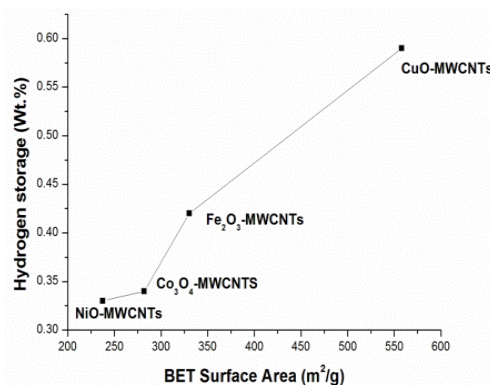


Fig. 7. Correlations of electrochemical hydrogen storage and BET surface area of 5wt.% CuO-MWCNTs, 5wt.% Fe_2O_3 -MWCNTs, 5wt.% NiO-MWCNTs and 5wt.% Co_3O_4 -MWCNTs.

4. Conclusions

XRD, TEM and TGA data has confirmed the presence of various metal oxides nanoparticles on the surface and within the walls of MWCNTs. The TGA profiles indicated that the structural stability of composites changes with metal oxides additions. The CuO-MWCNTs composite showed good hydrogen adsorption in relation to other metal oxides and A-MWCNTs. Interestingly, the hydrogen adsorption of CuO-MWCNTs correlated with higher BET surface area ($558.04 \text{ m}^2/\text{g}$) and increased mesopores. The discharge capacity values decreased as follows: 5wt.% CuO-MWCNTs > 5wt.% Fe_2O_3 -MWCNTs > 5wt.% Co_3O_4 -MWCNTs > 5wt.% NiO-MWCNTs. The crystallites sizes and morphology of metal oxides on MWCNTs played a

significant role in electrochemical storage of hydrogen. The discharge capacity data indicates the existence of synergy between Cu and MWCNTs towards electrochemical hydrogen storage.

Acknowledgements

The support of this work by SASOL Inzalo foundation and University of Limpopo (Turffloop Campus), Department of Chemistry is gratefully acknowledged. One of us (NB Mkhondo) would like to acknowledge the awarding of scholarship by SASOL Inzalo foundation.

References

- [1] S. M. Abbas, S. T. Hussain, S. Ali, K. S. Munawar, N. Ahmad, N. Ali, *Mater. Lett.* **107**, 158003).
- [2] K. Xie, J. Li, Y. Lai, W. Lu, Z. Zhang, Y. Liu, L. Zhou, H. Huang, *Electrochem. Commun.* **13**, 657 (2011).
- [3] A. Pendashteh, M. F. Mousavia, M. S. Rahmanifar, *Electrochim. Acta* **88**, 347 (2013).
- [4] S. Mallakpour, E. Khadem, *Chem. Eng. J.* **302**, 344 (2016).
- [5] L. Yang, J. Chen, X. Wei, B. Liu, Y. Kuang, *Electrochim. Acta* **53**, 777 (2007).
- [6] D-Y. Wang, M. Gong, H-L. Chou, C-J. Pan, H-A. Chen, Y. Wu, M-C. Lin, M. Guan, J. Yang, C-W. Chen, Y-L. Wang, B-J. Hwang, C-C. Chen, H. Dai, *J. Am. Chem. Soc.* **137**(4), 1587 (2015).
- [7] G. Xiong, K. P. S. S. Hembrama, R. G. Reifengerger, T. S. Fisher, *J. Power Sources* **227**, 254013).
- [8] S. Fan, X. Liu, Y. Li, E. Yan, C. Wang, J. Liu, Y. Zhang, *Mater. Lett.* **91**, 291 (2013).
- [9] E. Liu, J. Wang, J. Li, C. Shi, C. He, X. Du, N. Zhao, *Int. J. Hydrogen Energy* **36**, 6739 (2011).
- [10] D. H. Lee, M. Kang, S-M. Paek, H. Jung, *Electrochim. Acta* **217**, 132 (2016).
- [11] T. Gholami, M. Salavati-Niasari, *Int. J. Hydrogen Energy* **41**, 15141 (2016).
- [12] H. G. Shiraz, M. G. Shiraz, *Int. J. Hydrogen Energy* **42**, 11528 (2017).
- [13] S. U. Rather, *Int. J. Hydrogen Energy* **42**, 11553 (2017).
- [14] X. Yan, X. Tong, J. Wang, C. Gong, M. Zhang, L. Liang, *J. Alloys Comp.* **593**, 184 (2014).
- [15] Y. Zhang, H. Feng, X. Wu, L. Wang, A. Zhang, T. Xia, H. Dong, X. Li, L. Zhang, *Int. J. Hydrogen Energy* **34**, 4889 (2009).
- [16] C.-C Yang, Y. J Li, W. Chen, *Int. J. Hydrogen Energy* **35**, 2336 (2010).
- [17] N. B. Mkhondo, T. Magadzu, *Dig. J. Nanomater. Bios.* **9**(4), 1331 (2014).
- [18] A. D. Su, X. Zhang, A. Rinaldi, S. T. Nguyen, H. Liu, Z. Lei, L. Lu, *Chem. Phys. Lett.* **561-562**, 68 (2013).
- [19] A. I. Inandar, Y. Kim, S. M. Pawar, J. H. Kim, H. Im, H. Kim, *J. Power Sources* **196**, 2393 (2011).
- [20] J. Deng, L. Kang, G. Bai, Y. Li, P. Li, X. Liu, Y. Yang, F. Gao, W. Liang, *Electrochim. Acta* **132**, 127 (2014).
- [21] S. M. Abbas, S. T. Hussain, S. Ali, N. Ahmad, *Electrochim. Acta* **105**, 481 (2013).
- [22] D. P. Dubal, G. S. Gunda, R. Holze, C. D. Lokhande, *J. Power Sources* **242**, 687 (2013).
- [23] L. Wang, L.-C. Zhang, J.-X. Cheng, C.-X. Ding, C.-H. Chen, *Electrochim. Acta* **102**, 306013).
- [24] C. Xu, B. Li, H. Du, F. Kang, Y. Zeng, *J. Power Sources* **180**, 664 (2008).
- [25] S. Zhang, P. Chuang, K. C. Ng, G. Z. Chen, *Electrochim. Acta* **55**, 7447 (2010).
- [26] J. Shen, A. Liu, Y. Tu, H. Wang, R. Jiang, J. Ouyang, Y. Chen, *Electrochim. Acta* **78**, 122 (2012).
- [27] Z. Fan, J. Chen, K. Cui, F. Sun, Y. Xu, Y. Kuang, *Electrochim. Acta* **52**, 2959 (2007).
- [28] C. Shan, H. Yang, J. Song, D. Han, A. Ivaska, L. Niu, *Analytical Chemistry* **81**, 2378 (2009).
- [29] C. Hsieh, Y. Chou, J. Lin, *Int. J. Hydrogen Energy* **32**, 3457 (2007).
- [30] H. Huang, K. Huang, S. Liu, S. Zhuang, D. Chen, *Mater. Sci.* **44**, 4460 (2009).